Pure Appl. Geophys. 167 (2010), 437–453

DOI 10.1007/s00024-010-0080-6

Pure and Applied Geophysics

The Temporal Morphology of Infrasound Propagation

Douglas P. Drob,[1] Milton Garcés,[2] Michael Hedlin,[3] and Nicolas Brachet[4]

Abstract—Expert knowledge suggests that the performance of automated infrasound event association and source location algorithms could be greatly improved by the ability to continually update station travel-time curves to properly account for the hourly, daily, and seasonal changes of the atmospheric state. With the goal of reducing false alarm rates and improving network detection capability we endeavor to develop, validate, and integrate this capability into infrasound processing operations at the International Data Centre of the Comprehensive Nuclear Test-Ban Treaty Organization. Numerous studies have demonstrated that incorporation of hybrid ground-to-space (G2S) enviromental specifications in numerical calculations of infrasound signal travel time and azimuth deviation yields significantly improved results over that of climatological atmospheric specifications, specifically for tropospheric and stratospheric modes. A robust infrastructure currently exists to generate hybrid G2S vector spherical harmonic coefficients, based on existing operational and emperical models on a real-time basis (every 3- to 6-hours) (Drob *et al.,* 2003). Thus the next requirement in this endeavor is to refine numerical procedures to calculate infrasound propagation characteristics for robust automatic infrasound arrival identification and network detection, location, and characterization algorithms. We present results from a new code that integrates the local (range-independent) τp ray equations to provide travel time, range, turning point, and azimuth deviation for any location on the globe given a G2S vector spherical harmonic coefficient set. The code employs an accurate numerical technique capable of handling square-root singularities. We investigate the seasonal variability of propagation characteristics over a five-year time series for two different stations within the International Monitoring System with the aim of understanding the capabilities of current working knowledge of the atmosphere and infrasound propagation models. The statistical behaviors or occurrence frequency of various propagation configurations are discussed. Representative examples of some of these propagation configuration states are also shown.

[1] Space Science Division, Naval Research Laboratory, Washington, DC, USA. E-mail: douglas.drob@nrl.navy.mil

[2] Infrasound Laboratory, University of Hawaii, Manoa, USA. E-mail: milton@isla.hawaii.edu

[3] Laboratory for Atmospheric Acoustics, University of California, San Diego, USA.

[4] International Data Centre, Provisional Technical Secretariat, CTBTO, Vienna, Austria.

Key words: Infrasound, atmospheric variability, climatology, automated event detection, source location, CTBTO, IDC, IMS.

1. Background

The purpose of the automated infrasound processing developed at the IDC is to detect coherent signals measured on individual IMS sensors (Christie *et al.,* 2001), highlight the most significant detections as "phases" (as opposed to "noise"), and subsequently group these phases to form and locate hypocenters, so-called "events". The phases are determined using the progressive multi-channel correlation (PMCC) method (Cansi, 1995) which distinguishes the coherent signals produced by natural and man-made sources from incoherent ambient background noise which may also be of natural, cultural, or instrumental origin. A wide variety of sources are regularly recorded worldwide by the IMS network; ocean activity, mountain associated waves, volcanic eruptions, earthquakes, thunderstorms, meteors, avalanches, auroras, rocket launches and reentries, aircraft, mine-blasts, accidental explosions, and industrial noise. It is important for the IDC to detect, locate, and categorize these sources to contrast with nuclear explosions; the task of the organization.

The detection, location, and characterization algorithms (henceforth DLC) described by Brown *et al.*, (2002a) may be used to locate the terminal burst point of exploding meteors, the origin time of volcanic eruptions, and the location of avalanches and rock slides, as well other null sources relevant to CTBTO operations (Le Pichon *et al.*, 2008b; Hedlin *et al.*, 2002). Although the various natural events represent false alarms for the CTBTO, they also provide valuable ground-truth information that can be

used to constantly fine-tune and check the integrity of the system, insuring verifiability of the treaty. For example, terminal bursts of meteors with an average yield of one kiloton occur in the earth's atmosphere several times per year (Nemtchinov *et al.*, 1997; Brown *et al.,* 2002b).

To facilitate rapid computation, today's automated DLC algorithms rely upon precompiled station travel-time information (Brown *et al.,* 2002a). The precompiled information, which is typically average propagation velocity and azimuth deviation, describes how an observed signal was affected by the background environment on its way from source to receiver. The application of this knowledge provides improved source location and signal association estimates.

Our objective is to reduce IDC false alarm rates and improve detection capability by reducing the sources of uncertainty in the existing model physics and DLC methodologies. Analyses of ground-truth events have shown that observationally constrained atmospheric specifications are superior to average climatology (Le Pichon *et al.,* 2002, 2005; Herrin *et al.,* 2006). This is particularly true for tropospheric and stratospheric propagation for which there are several global operational numerical weather prediction systems such as the NOAA Global Forecast System (Kalnay *et al.,* 1990) and ECMWF (Courtier *et al.,* 1998; Bechtold *et al.,* 2008). Unfortunately, these systems are currently limited in their altitude extent due to the unavailability of routine operational satellite observations above approximately 80 km. The ground-to-space (G2S) environmental specification system was therefore developed to provide a compact numerical weather prediction post-processor and infrasound propagation calculation preprocessor (Drob *et al.,* 2003) to account for all altitudes pertinent to infrasound propagation. The system serves as a placeholder until operational numerical weather prediction models and data sets include the lower thermosphere.

In addition to requiring up-to-date knowledge about the atmospheric state for improving DLC algorithms, an acoustic wave propagation model is required to compute how observed infrasound signals relate back to their source. In discrete inverse theory (Menke, 1989) this is known as a forward model. There are a number of propagation modeling techniques available such as ray tracing (Gossard and Hooke, 1975), parabolic equations (Lingevitch *et al.,* 2002), and normal modes (Pierce, 1967). Unfortunately with detailed physics comes greater complexity. The approach must not be so primitive that any value added from near-real-time atmospheric specification has no meaningful influence; in turn, the technique must not be so complicated that implementation is impractical in automated DLC algorithms. The data and procedures must be readily available and simple enough to integrate into operational monitoring systems.

2. The τp Equations

At present the τp equations of Garces *et al.,* (1998) provide a good balance of simplicity and geophysical information content for automated DLC algorithms, particularly in conjunction with near-real-time atmospheric specifications. In general, the acoustic ray-tracing approach represents the propagation or translation and rotation of an acoustic wavefront through space and time. The τp equations are an expression of the Eikonal ray-tracing equations (Lighthill, 1978; Gossard and Hooke, 1975) in integral form with the approximations of range independence and no vertical wind. For this, each ray or wavefront element can be uniquely represented by an invariant ray parameter (p),

$$p = \frac{k_z}{c_o}\left(1 + \frac{k_z u_o}{c_o}\right)^{-1}, \tag{1}$$

which depends on the static sound speed at the receiver (c_o), the vertical wave number $k_z = \sin(q)$ where q is elevation angle, and u_o the horizontal wind velocity along the direction of propagation at the receiver. This ray parameter is also the reciprocal of the intrinsic horizontal phase velocity of the wave $V_\theta = 1/p$, therefore;

$$V_\theta = \frac{c_o}{k_z}\left(1 - \frac{k_z}{c_o}\right). \tag{2}$$

The equation for the along track range travelled between bounces, i.e., propagation from the bottom of the atmospheric duct to the top and back down again in a phase loop is

$$R(z,p) = 2\int_{z_o}^{z(p)} \psi(z,p)\left[\frac{p}{(1-u(z)p)} + u(z)\zeta(z)\right]dz, \tag{3}$$

where z_o is the lower limit of integration (typically zero or the surface altitude) and $z(p)$ is the upper limit, which is the first root above z_o of the characteristic function.

$$\psi(z,p) = \left[\zeta(z) - \frac{p^2}{(1-u(z)p)^2}\right]^{-1/2}. \tag{4}$$

This root represents the turning point of the ray following from classical WKB ray theory which states that a ray will turn when its horizontal phase velocity (V_θ) matches that of the background effective sound speed, $c(z) + u(z)$ where these are the adiabatic sound velocity and horizontal wind speed along the direction of propagation, respectively. The infrasound propagation characteristics in Eqs. 3 and 4 are a function of the local vertical profiles of $\zeta(z) = 1/c^2(z)$ and $u(z)$ as well. The corresponding travel time (T) for a phase loop is similarly

$$T(z,p) = 2\int_{z_o}^{z(p)} \psi(z,p)\zeta(z)dz. \tag{5}$$

The celerity (V), or average group velocity from the source to the receiver is simply $V = R/T$. Lastly, the apparent azimuth deviation is computed as $\Omega = \arctan^{-1}(Q/R)$ where the transverse offset (Q) for a phase loop is

$$Q(z,p) = \int_{z_o}^{z(p)} \psi(z,p)\zeta(z)v(z)dz, \tag{6}$$

where $v(z)$ is the horizontal wind component transverse to the direction of propagation. Throughout this paper, all of the results are computed in the frame of reference of the receiver as opposed to the source by simply reversing the sign of the wind fields. It can be shown that this is also equivalent to integrating the Eikonal ray equations in differential form with a negative time step.

A discussion of the methodology for the estimation of the eigenrays associating a received signal with a given source is beyond the scope of the present work. Relevant, however, is the fact that for a specific eigenray the measured azimuth deviation is an apparent effect similar to that of an airplane yawing in a crosswind in order to maintain a constant bearing. The acoustic wavefront must be skewed at some angle Ω with respect to the great circle path in order to offset the net lateral advection from transverse wind components; in other words so that the net transverse offset at the top and bottom of the phase loop are zero. Although the total path does not deviate from the true great circle path between source and receiver, in the presence of transverse winds the wavefront can depart from the great circle path anywhere else in the phase loop. Over one range of altitudes a crosswind may push the ray off the great circle path, while at other altitudes a crosswind in the opposite direction may push the ray back onto the great circle path. Furthermore, the ray may deviate to one side of the path on the up leg and the other side of the path on the down leg. This is also an important factor that needs to be considered when signals are observed from a source at altitude such as a bolide. Care must be taken in automated and interactive DLC algorithms when applying calculated values of Ω to correct the array observations for apparent azimuth deviation. If topography and atmospheric range variations are included then the actual path can be even more complicated, however the overall characteristics remain the same.

The crux of solving the τp integrals accurately is the treatment of the inverse square-root singularity in the function $\psi(z)$ at the upper limit of the domain. At any point in the domain (i.e. for any given p) the root is calculated by first bracketing it with a grid search and then applying Brent's method to approximate the root to a high degree of accuracy (Press, 1989). Knowing the location of the square-root singularity $z(p)$, Eqs. (3)–(6) can then be integrated with a Romberg method employing a modified midpoint rule that can handle inverse square-root singularities at the upper bound (Press, 1989). For all of the numerical results presented, continuous functional values for $u(z)$, $w(z)$, $c(z)$, and $\zeta(z)$ are calculated by cubic spline interpolation of gridded G2S values with $\Delta z = 125$ m. Note that the calculation of vertical derivatives is not required to integrate Eqs. (3)–(6).

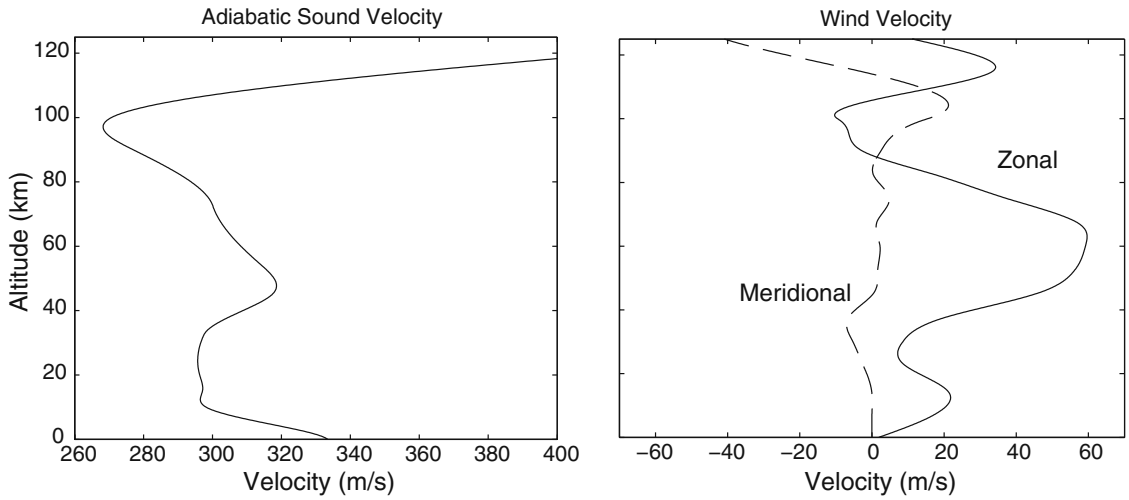

Figure 1
Climatological profiles; adiabatic sound velocity (*left*), zonal wind (*right solid*), and meridional wind (*right, dashed*) from the HWM93/MSISE-00 empirical models (Hedin *et al.,* 1996; Picone *et al.,* 2002) for January 1, 2005 at 00:00 UT

These integrals may also be evaluated for sources at altitude such as bolides by including a second term for the fractional part of the propagation phase loop where the limits of integration have been adjusted accordingly.

Two factors are relevant to current IDC DLC processing with respect to signals generated by sources well above the ground where the expected number of detectable phases can double at distant recording stations owing to the fact that a source will have both upward and downward directed acoustic components. First, current automated procedures focus on picking the onset time of the fastest infrasound arrival, and when and where closely spaced multiple arrivals exist, they tend to be averaged into a single characteristic by the parameters of the automated PMCC feature extraction algorithms. Secondly, progress has been made to demonstrate that it is possible to estimate hypocenter altitude at the level of interactive IDC analyst expert review, where manual identification of tropospheric, stratospheric, and thermospheric phases is possible; and in particular in conjunction with additional information from detections by the seismic, and auxiliary seismic components of the IMS network (Edwards and Hildebrand, 2004; Arrowsmith *et al.,* 2007; Le Pichon *et al.,* 2008a). As experience progresses, it will eventually be possible to implement these considerations into automated IDC processing, however as is the case in seismology, hypocenters depths are difficult to compute without a dense local network or specific depth phases. Automated hypocenter height estimates via infrasound will thus likely only be approximate until an IDC analyst can refine them.

Example climatological profiles from the HWM93/MSISE-00 empirical models (Hedin *et al.,* 1996; Picone *et al.,* 2002) for January 1, 2005 at 00:00 UT for a typical northern hemisphere mid-latitude station (I56US) are shown in Fig. 1. Illustrative τp calculations corresponding to these example profiles are shown in Fig. 2. These calculations are performed over all observable azimuths for elevation angles from 0° to 35°. The horizontal phase velocity (V_θ) of the parameter space over the domain is shown in panel A. Recall that this is only a function of the atmospheric conditions at the detector. Panel B shows a contour plot of the effective sound velocity as a function of altitude (z) and backazimuth. The wintertime stratospheric wind jet near 55 km can be observed, with winds toward the detector at −90°, and away from the detector at +90°. The turning points of all incoming rays at elevation angles of 5°, 10°, and 15° are also indicated. The corresponding turning heights of the rays, over the entire domain, is shown in panel C. Two predominant ducts are present at this time and location, the thermospheric duct for all backazimuths and the eastward stratospheric duct from the wintertime stratospheric zonal wind jet. The

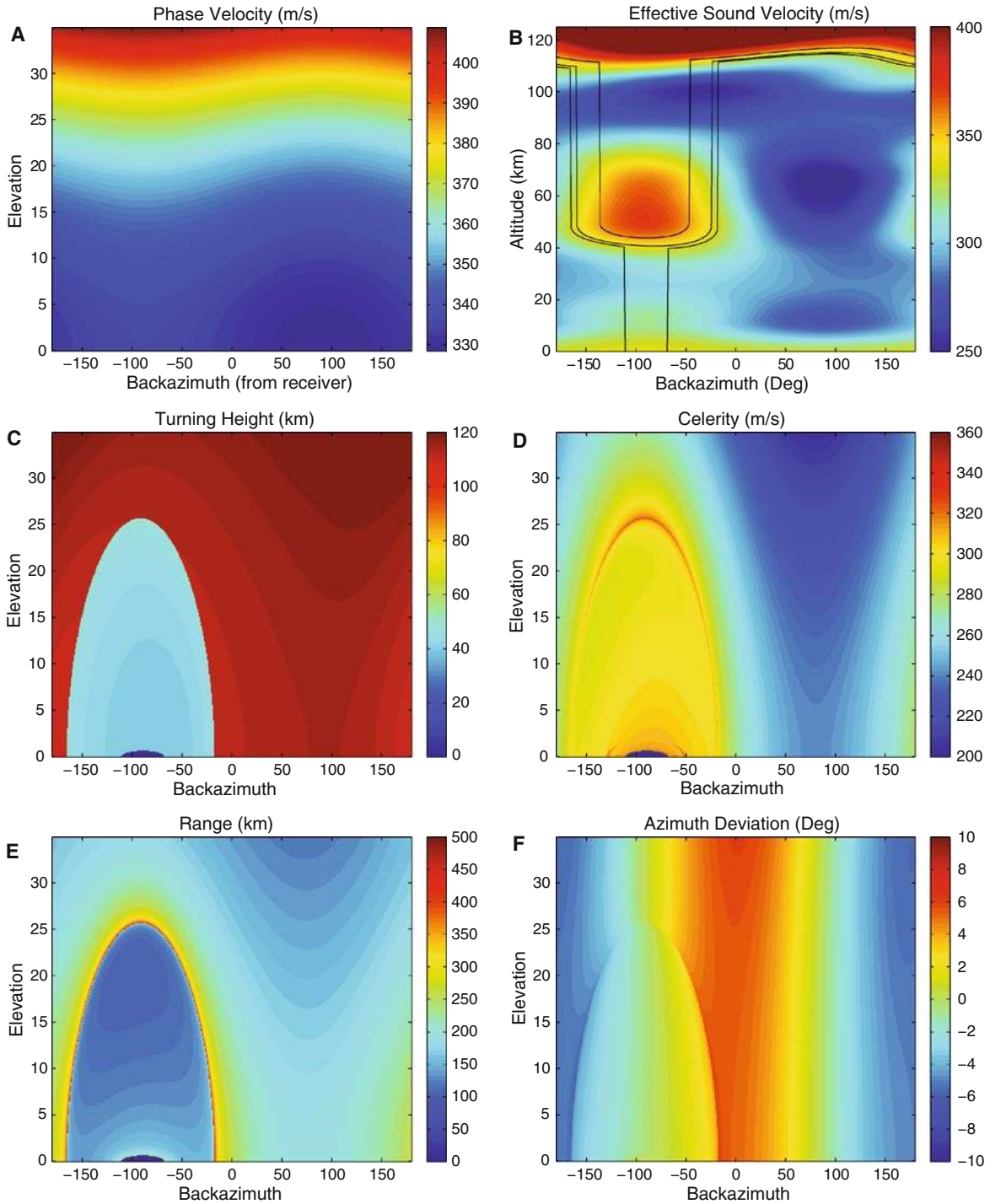

Figure 2

τp ducting characteristics for I56US (48.2640°N, 117.1257°W) on January 1, 2006 0:00 UTC as function of backazimuth at the detector. Panel A show the horizontal phase velocity for all elevations from 0° to 35°, Panel B shows the effective sound speed velocity in the direction of propagation, Panel C the ray turning height, panel D the celerity, and E the range to first bounce, and F the apparent azimuth deviation. The contour lines in panel B indicate the turning height of rays launched at elevation angles of 5°, 10°, and 15°, respectively

dark blue area represents a region where the acoustic energy is immediately refracted downward toward the earth's surface by the ambient atmospheric conditions. Panels D, E, and F show the celerity (V), range (R), and apparent azimuth deviation (Ω) over the computational domain, respectively. A very stable and accurate result can be obtained over the entire domain, including in the vicinity of the cusp regions where fast propagation modes exist (Evers and Haak, 2007). These fast modes can be seen near the transition from the stratospheric to the thermospheric ducts for look directions to the west.

Several limitations resulting from the various approximations in the τp method such as the shortcomings of linear ray-tracing theory (Millet *et al.,* 2007), the lack of explicit range dependence (Drob *et al.,* 2003), and the influence of internal scattering by internal gravity waves (Chunchuzov, 2004; Ostashev *et al.,* 2005) are noteworthy but beyond the scope of the present discussion. With the doubling of processing capacities every few years following Moore's Law, more complex calculations that account for range-dependent variations in the background atmosphere should be investigated and eventually implemented in automated DLC algorithms. The objective at hand is to provide geophysical insight to demonstrate that the utilization of climatological travel times in DLC algorithms is at best outdated in comparison to the possibility of calculating them in real time following from recent progress in atmospheric specification and infrasound propagation codes.

3. Results

Classic pioneering work by Georges and Beasley, (1977) and others, which relied on limited knowledge of the atmosphere, developed an appreciation for how infrasound ducting characteristics vary with latitude over the year. With more recent information from thirty-five years of satellite and ground-based atmospheric wind and temperature measurements, Drob *et al.,* (2003) investigated how infrasound propagation characteristics varied over the globe at a given universal time; in particular, how acoustic energy is partitioned between the troposphere, stratospheric, and thermosphere ducts. To provide some context, Fig. 3 shows the global distribution of infrasound ducting characteristics for an arbitrary time of 05/24/2006 00:00 UT. For a particular altitude level, each global map represents the fraction of acoustic energy from an isotropically radiating acoustic point source on the ground, summed over all possible propagation directions (see Drob *et al.,* 2003).

The regions where tropospheric ducting occurs are shown in the top panel. Ducting along the tropospheric jet stream can also be seen in the Southern Hemisphere. Marine inversion layers also occurred off the west coast of California and Africa, as well as near the Korean Peninsula. Stratospheric ducting (middle panel) is seen in the Northern And Southern Hemisphere mid-latitude regions but is absent in the equatorial regions. The lower panel shows the remaining thermospheric ducting fractions. Interesting correlations in the thermospheric ducting fractions with continental landmasses and lower atmospheric ducting fractions can also be seen. The inverse correlations between the upper and lower atmospheric ducting fractions are due to the fact that what was not ducted in the lower atmosphere can be ducted in the upper mesosphere and lower thermosphere.

Following the work of Drob *et al.,* (2003), we now present several case studies based on the calculation of a multiyear time series of infrasound propagation characteristics for two of the IMS infrasound stations; I56US a mid-latitude Northern Hemisphere station at (48.26°N, 117.13°W), and I55US a polar latitude Southern Hemisphere station at (77.74°S, 167.58°E). We compare and contrast the results calculated from both climatology (HWM93/MSISE-00) and hybrid G2S specifications. For these two IMS stations, we present a five-year long-time series from September 13, 2002 to April 30, 2007 at 6 h intervals (4× daily) of the infrasound ducting characteristics of ray turning heights z(p), celerity (V) and backazimuth (Ω). The later two have direct application in infrasound DLC algorithms.

In the detection algorithms described by Brown *et al.,* (2002a) currently in use at the IDC, backazimuths receive a slightly greater statistical emphasis (1.0) as compared to travel times (0.8) in the calculation of a metric (Σ) for the trigging of an automatic event ($\Sigma > 3.55$) and Reviewed Event Bulletin

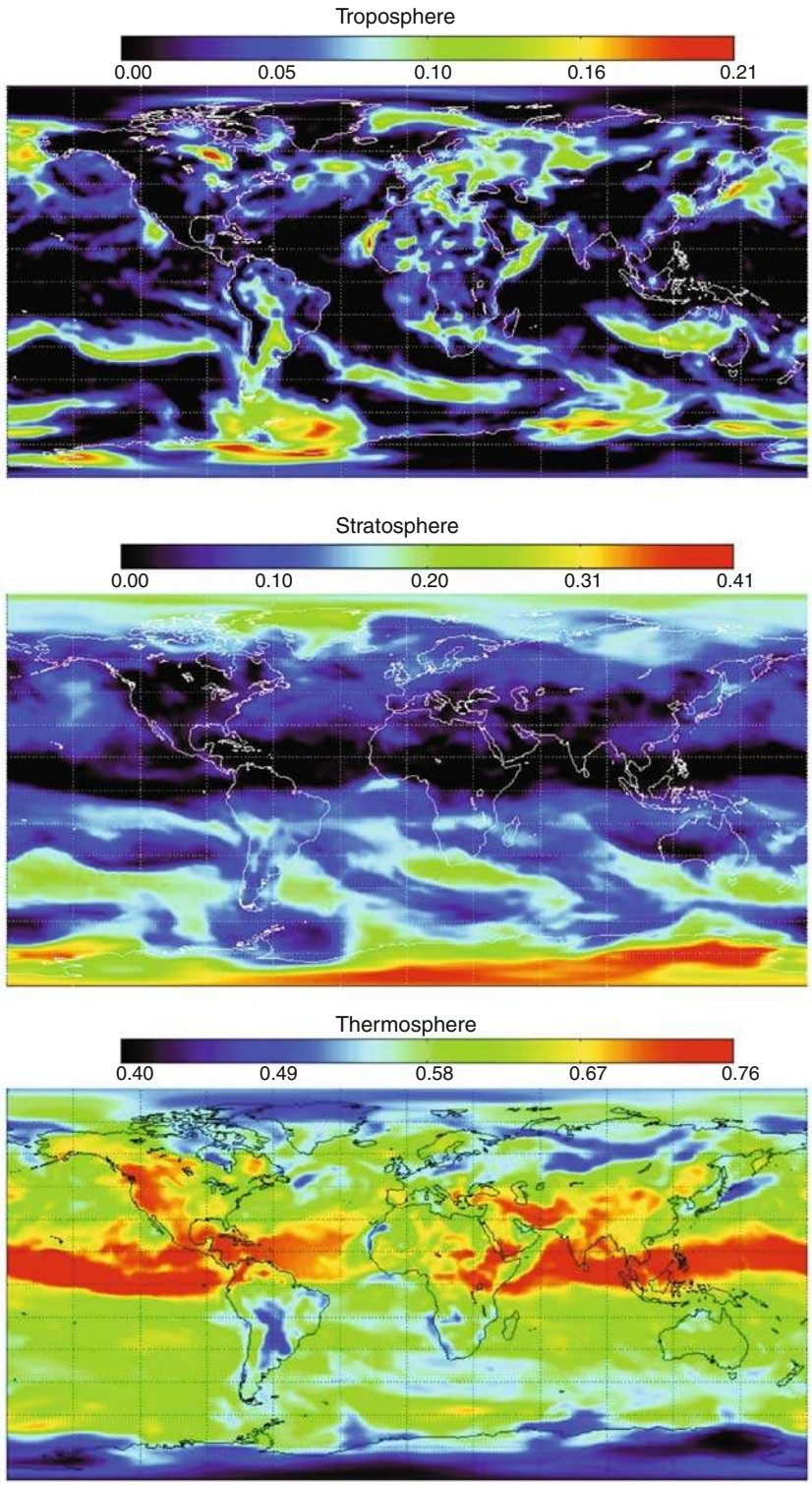

Figure 3
Tropospheric, stratospheric, and thermospheric infrasound ducting fractions for 05/24/2006 00:00 UT

(REB) ($\Sigma > 4.6$). This detection criteria effectively defines a significant event as one that can be established by at least two well-defined and intersecting back azimuths for which the associated travel times do not also violate causality (Brown *et al.,* 2002a). More recently, a novel detection scheme was developed by Arrowsmith *et al.,* (2008) that dynamically adjusts network detection thresholds in real time to account for the presence of correlated and varying background noise. Furthermore, Arrowsmith *et al.,* (2008) demonstrated that the new algorithm has excellent performance characteristics in the presence of clutter, suggesting the approach provides a viable means to reduce the number of false alarms that need to be reviewed by a human analysis. Neither approach currently accounts for the hourly, daily, or seasonal changes of the travel time or azimuth deviation resulting from the corresponding changes in the atmospheric conditions; the inclusion of which would further allow for a more accurate calculation of the Σ metric thus improving the network sensitivity and reducing the number of false alarms.

4. I56US

Figure 4 shows the computed turning points of infrasound for arrivals at I56US for an elevation of 5°. The top panel shows the results calculated from the climatology and the lower panel the results calculated with the hybrid G2S specification. The alternating seasonal pattern, where eastward stratospheric propagation is observed in the wintertime and westward stratospheric propagation is observed in the summer time, is evident. Ducting caused by the tropospheric jet stream for predominantly eastward propagating arrivals, as well as occasionally for northward and southward directions, can also be seen. Furthermore, occasional stratospheric ducting in both the westward and eastward directions, related to global-scale dynamical instabilities in the stratosphere, can sometimes occur during the winter months. As would be expected but not shown here, the corresponding results for lower elevation angles exhibit more tropospheric and stratospheric ducting for lower incoming elevations and less for large elevation angles (more thermospheric ducting).

Figure 5a shows the azimuth deviation for westward arrivals from the five-year time series at I56US; climatological values are indicated in red and results from the hybrid specifications in blue. There is an average scatter in the hybrid specifications of about ±2°, on par with the climatological predictions, plus occasional excursions of up to ±4° during the winter months. The four interleaved bands in the climatologically predicted variations result from the different local times under the influence of the solar migrating tides as described by Garces *et al.,* (1998). Figure 5b shows the azimuth deviation for southward arrivals with excursions up to 10° in January 2003, and on average up to 7.5° during wintertime. In addition, there is an asymmetry with respect to the summer months with deviations of up to −3°, which tend to be more stable. These wide ranging azimuth deviations result from the annual variations of the stratospheric wind jet which is predominantly eastward, lower, stronger, and variable in the wintertime, as compared to the summertime jet which is westward, higher, and stable.

Figure 6a shows a time series of celerity for I56US for eastward arrivals again at 5° elevation, calculated with hybrid G2S and empirical atmospheric specifications. A band of arrivals at 340 m/s, which are comprised of both lower tropospheric, upper tropospheric, and even stratospheric modes, is evident. Random departures of up to 30 m/s from climatological estimates and seasonal variations occur during wintertime for the other branch of arrivals between 250 and 320 m/s.

Figure 6b presents the comparison of celerity for all southward arrivals at 5° elevation. Note the occasional tropospheric modes (330 m/s) with a half-width of 20 m/s, including seasonal oscillations. The predicted tidal oscillations are also more significant. With respect to the climatology, lower atmospheric ducting to the north and south are generally not expected as the meridional wind fields average to zero over the globe.

Figure 6c shows the results for westward arrivals. Of note is the presence of occasional tropospheric arrivals (340 m/s) with clear seasonal variability. If not properly accounted for (i.e. given the appropriate statistical weighting) these could result in spurious associations and poor source localizations. The results also show that there is pronounced annual variability

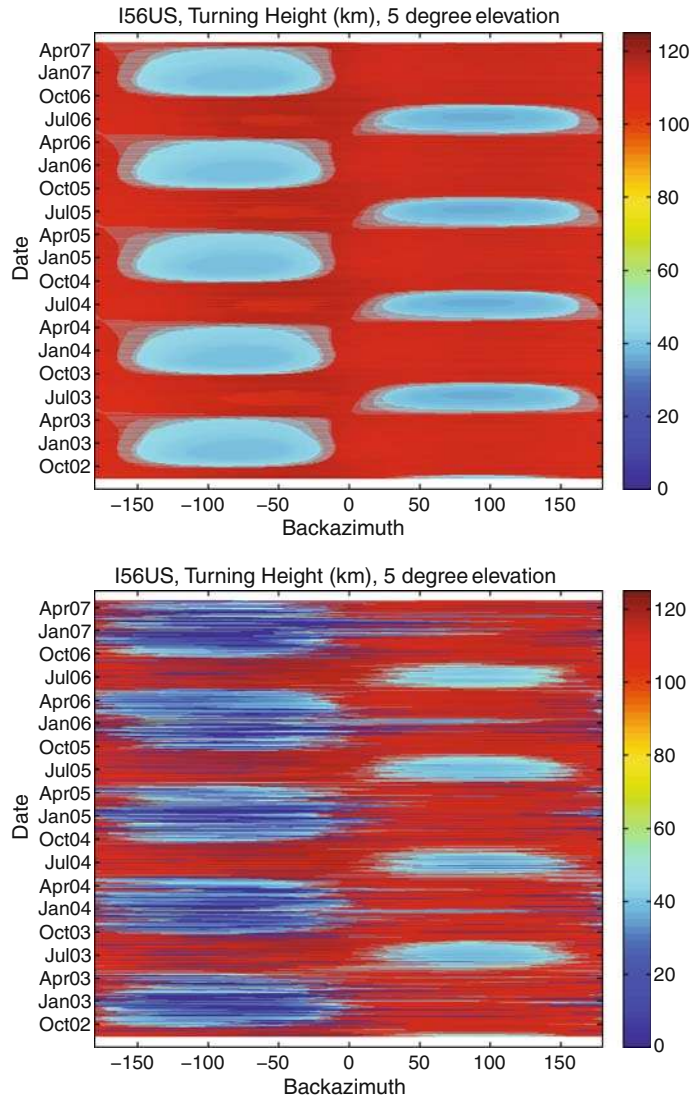

Figure 4
The turning height for all rays at I56US that enter the receiver at an elevation angle of 5°. The upper panel shows the results calculated from the HWM/MSIS climatology and the lower panel the results from the hybrid G2S atmospheric specifications

with stable stratospheric modes in the summer time, transitioning to thermospheric modes in the wintertime as was shown in Fig. 4. The existence of sporadic stratospheric modes occurring in both the eastward and westward directions in late winter are associated with the dynamical instability of the stratospheric wind jet driven by vertically propagating planetary waves. Disturbances associated with sudden stratospheric warmings (Manney *et al.,* 2008) can even result in prolonged intervals of westward winds in the stratosphere during the wintertime.

5. I55US

The second set of illustrative examples is for the polar Southern Hemisphere station I55US. The comparison of turning points calculated with climatology and the hybrid specifications for rays that will enter the detector at 5° elevation, as a function of backazimuth and time, are shown in Fig. 7. While the overall morphology of the climatological and hybrid specifications for the mid-latitude I56US station is generally similar in Fig. 4, this is not the case for

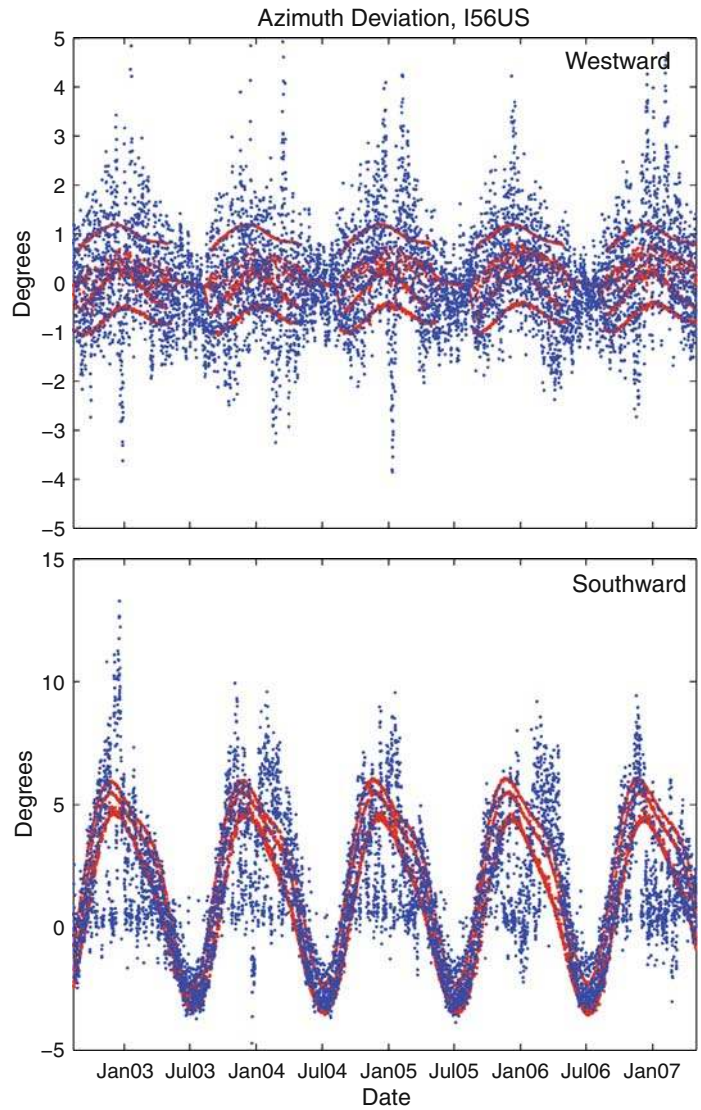

Figure 5
Time series of azimuth deviation of westward (*top*) and southward (*bottom*) arrival for I56US at an elevation angle of 5°. Predictions using climatology are in red. Predictions using the hybrid (G2S) model are in blue

I55US. Again, the day-to-day variability, whether for a tropospheric, stratospheric, or thermospheric duct, is more pronounced in the real atmosphere (G2S hybrid) than the calculations with the monthly average climatology would imply. From these examples it should be obvious that climatology does not accurately predict the occurrence of tropospheric and even stratospheric ducting in the region.

The time series of computed celerity for westward arrivals is shown in Fig. 8a. Annual variations of hybrid G2S characteristics follow the climatology of the predominate stratospheric and thermospheric modes reasonably well, but not perfectly. Like for the Northern Hemisphere mid-latitudes, greater variability exists in the computed propagation characteristics during wintertime. A predominant but transient lower atmospheric mode, disappearing in summer, with an

Figure 6 ▶
Time series of the celerity for 5° elevation arrivals at I56US for eastward, southward, and westward directions, respectively. The color coding is as described in the caption for Fig. 5

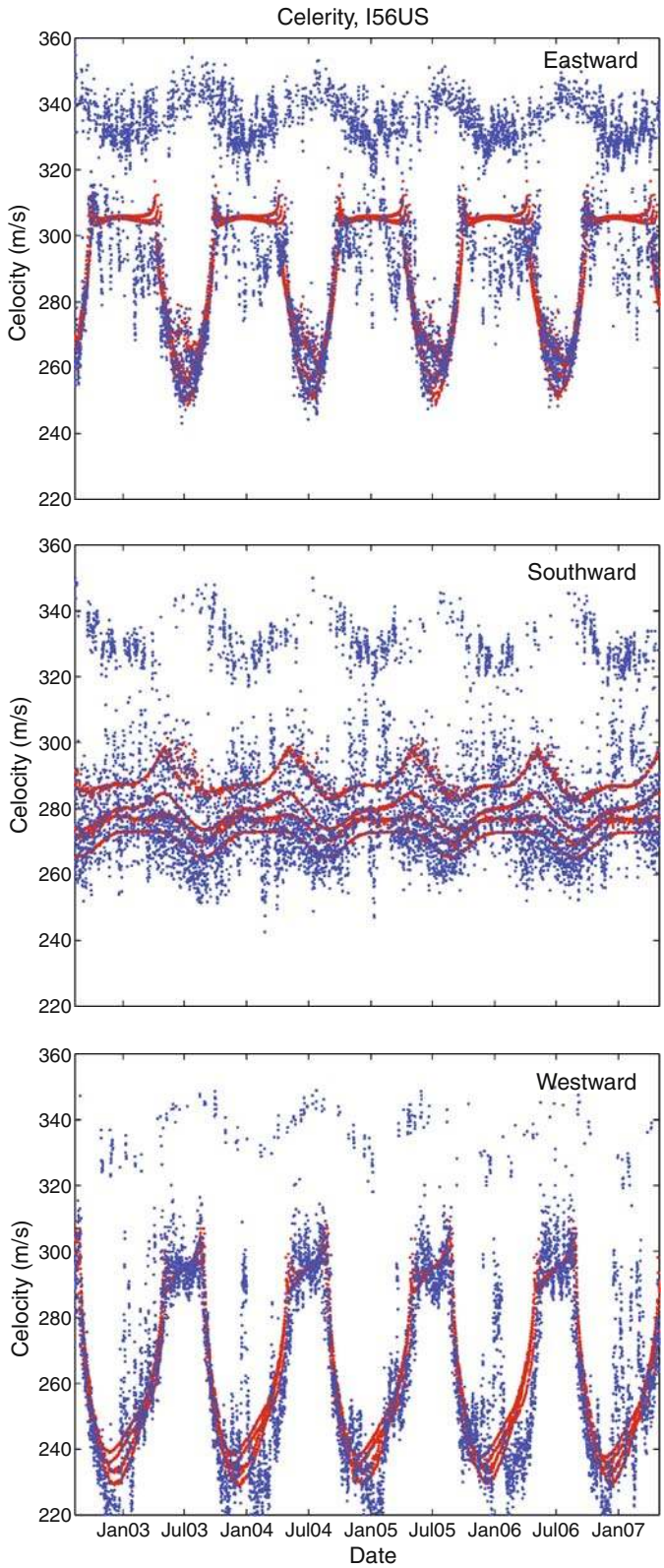
Celerity, I56US
Eastward
Southward
Westward
Celocity (m/s)
360
340
320
300
280
260
240
220
Jan03
Jul03
Jan04
Jul04
Jan05
Jul05
Jan06
Jul06
Jan07
Date

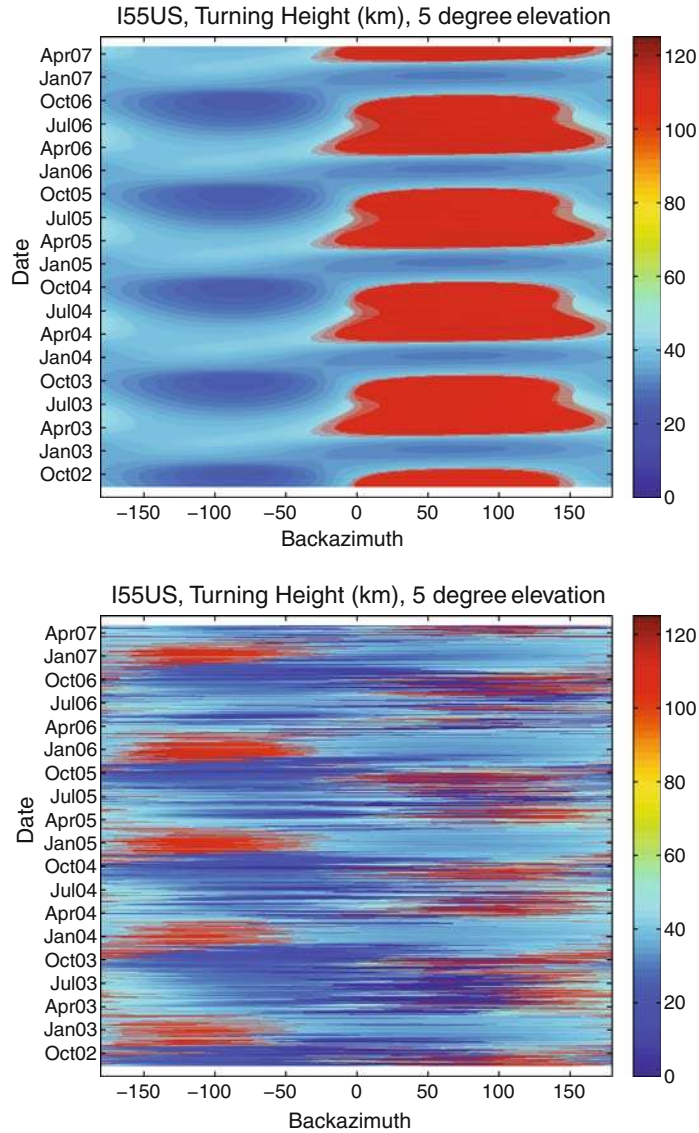

Figure 7
The turning height for all rays at I55US that enter the receiver at an elevation angle of 5°. The upper panel shows the results calculated from the HWM/MSIS climatology and the lower panel the results from the hybrid G2S atmospheric specifications

average celerity of about 310 m/s is also present. The 340 m/s celerities observed at I56US (Fig. 6) are generally not be observed at I55US as the polar troposphere is colder and the station is too far poleward to be influenced by the tropospheric jet stream. Figure 8b shows the results for southward arrivals, which vary from 260 to 325 m/s, again exhibiting significant departures from climatological predictions.

Lastly, we consider the azimuth deviations for IMS station I55US. The time series of southward arrivals is shown in Fig. 9a, for which there are asymmetric seasonal variations with occasional sporadic excursions of over 10°, and up to 7.5° on average. Significant local-time (tidal) variations of the thermospheric modes are again present in the climatology. The results shown in Fig. 9b for the westward

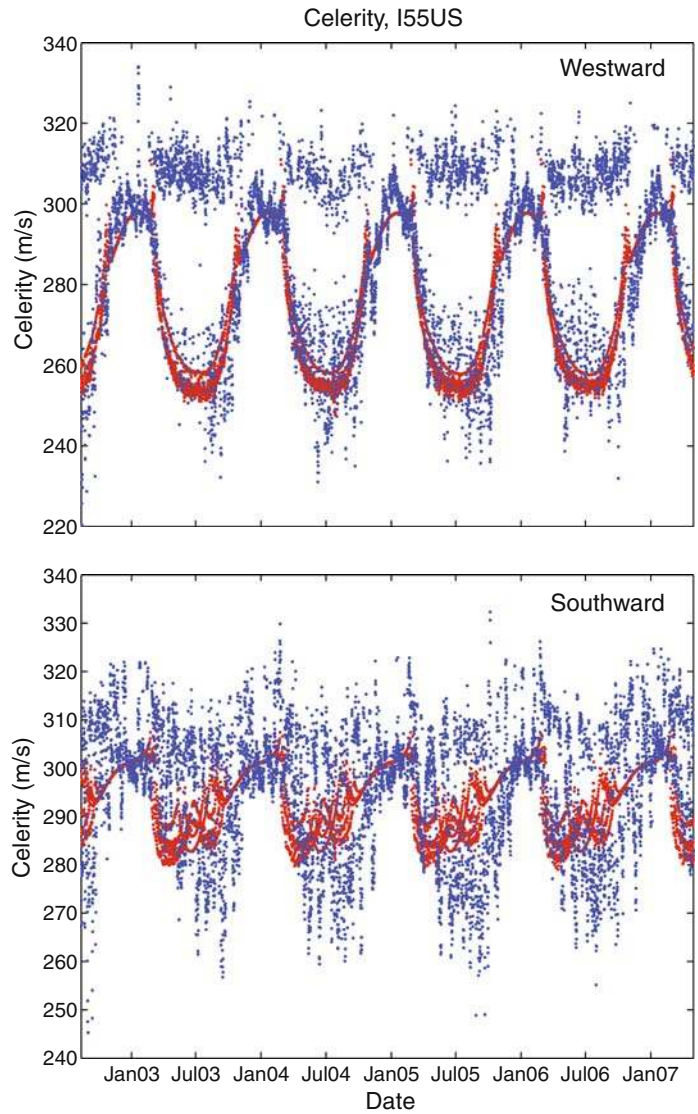

Figure 8
Time series of the celerity for 5° elevation arrivals at I55US for westward and southward, respectively. The color coding is as described in the caption for Fig. 5

arrivals at I55US depart widely from the average climatology going from +4° to −4° over a month.

6. Discussion/Conclusion

As described in Brown *et al.,* (2002a) one could imagine tables of statistical propagation characteristics comprised of several dominant modes that could be implemented in operational DLC algorithms; a constant phase at 310–340 m/s and an annual varying one with stratospheric and thermospheric phases. In future IDC software updates, these could and should also be a function of day of the year, look direction, and station. Histogram analysis could be used to establish preferred propagation modes with uncertainties and assigned probabilities based on half-widths; however, direct utilization of the procedures we have outlined here on a daily basis is just as easy to implement. At present the IDC uses travel-time tables which are independent of season, though do depend on the elevation of arrival.

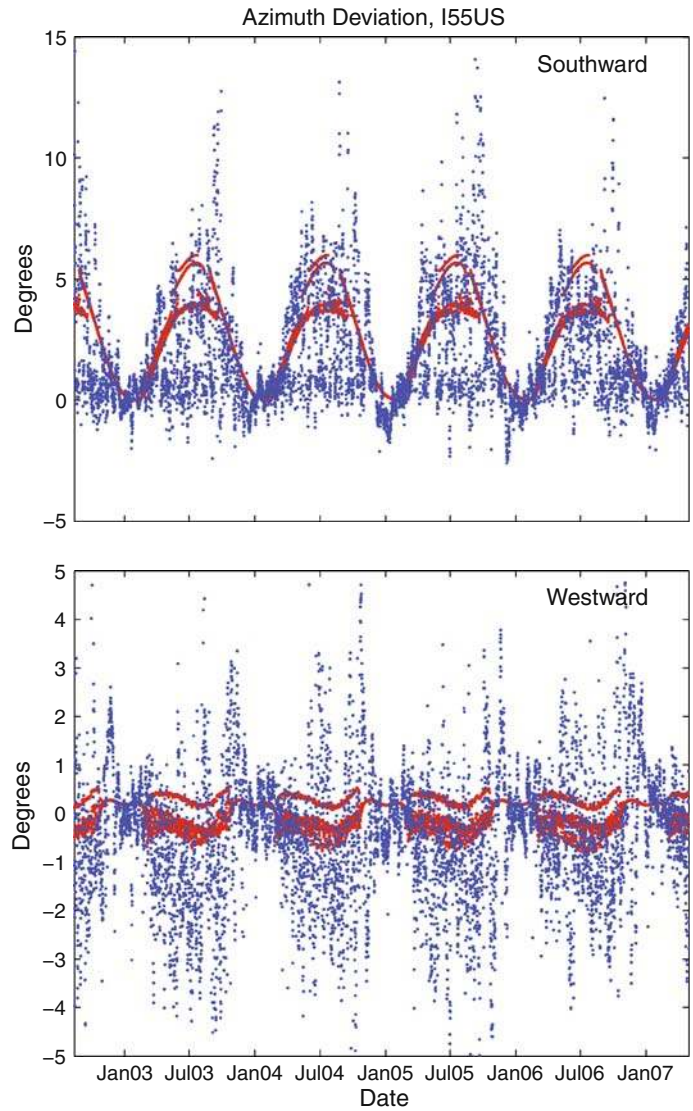

Figure 9
Time series of southward and westward arrivals for I55US at an elevation angle of 5°, respectively. The color coding is as described in the caption for Fig. 5

Furthermore, from the consideration of the variability of backazimuth and celerity presented, it is clear that the current seasonal averaged travel-time tables provide a poor representation of the day-to-day and month-to-month variations, and thus limit the full potential of the CTBTO automated infrasound DLC algorithms. The inherent variability is simply lost in the histogram analysis. It should be noted that in concert with the other monitoring technologies of the CTBTO, the current infrasound algorithms are passable, but improvable, as has been demonstrated by numerous researchers and results. Additional work, following examples such as Arrowsmith *et al.,* (2008); Le Pichon *et al.,* (2008c) should be undertaken in order to ascertain the value added to the system in terms of false alarm rates and network detection thresholds with careful consideration of the computational complexity and burden introduced into the existing operational system.

With respect to caveats for the calculations presented here, for certain locations and times the dynamical variability of the upper mesospheric and

lower thermospheric modes may be even greater in reality than calculated here after accounting for observed and documented non-migrating tides (Forbes *et al.,* 2003), day-to-day and inter-seasonal tidal variability (Fritts and Isler, 1994; Lieberman *et al.,* 2007), and the existence of vertically propagating and stationary mesosphere lower thermosphere planetary waves (Smith, 1996; McLandress *et al.,* 2006) above 55 km. These effects are not yet fully included in either the empirical climatology or hybrid G2S atmospheric specification. The HWM93 model is also known to underestimate the magnitude of the migrating tides for certain seasons and latitudes. A recent update of HWM (HWM07) by Drob *et al.,* (2008) resolves most of the issues related to the amplitude and phases of the migrating solar tides in the mesosphere and lower thermosphere. Given a proper statistical treatment of the present uncertainties, limitations of the present atmospheric specifications above 55 km should not invalidate the applicability of the work described here to DLC algorithms. In particular, tropospheric and stratospheric modes, which have a much greater signal to noise ratio are more likely to be detected and not subject to these problems.

The τp and G2S software which produced the results presented here are specifically designed to be utilized at the IDC in batch mode via a shell script in order to compute the local propagation characteristics for all IMS infrasound stations in real time. These codes can also be invoked interactively by an IDC analysist. For a given station and time the τp calculations only require a few seconds to complete. The process is relatively fast compared to the periodic calculations of the global G2S coefficient set from available atmospheric data sources, requiring several minutes to downloading available global weather fields and perform the vector spherical harmonic transforms. With the addition or allocation of a single dedicated compute node that is accessible to the operational DLC system, the travel-time characteristics for all sixty IMS infrasound stations could be updated every 60 min. Compared to automated DLC calculations from climatological travel-time tables gains in system performance could thus be achieved.

Recent ground-truth events investigated by the infrasound research community have clearly demonstrated that accurate atmospheric specifications are required to properly explain observed infrasound signals. In tandem, the atmospheric science community is continually improving and currently producing reliable specifications of the atmospheric state that can be utilized to improve automated DLC algorithms. Given the advances and availability of low-cost computing resources, and the reliable openly available real-time atmospheric specifications such as provided by NOAA and ECMWF there are no good reasons, technical or otherwise, why near-real-time travel-time tables should not be used in infrasound propagation calculations. Of course when these systems are brought online it is important to continually monitor and evaluate the performance with the many naturally occurring geophysical, as well as coincidental man-made, ground-truth events. One possibility as already demonstrated by similar research is the example of the analysis of the multi-year time series of volcanic observations at I22FR (Le Pichon *et al.,* 2005). Lastly for robust event location and screening of automated event bulletins by human analysts (Brown *et al.,* 2002a), we recommend that detailed propagation modeling techniques that account for range dependence (Gossard and Hooke, 1975), topography (Arrowsmith *et al.,* 2007), and other effects such as interval gravity waves (Ostashev *et al.,* 2005; Chunchuzov, 2004) be utilized.

This paper has presented time series of infrasound propagation characteristics. A number of physical approximations where made to keep these calculations simple and robust. Through these calculations, we have argued that precomputed monthly average travel-time tables are poor for operational DLC algorithms. To this end, we have advanced progress toward the integration of real-time infrasound propagation travel-time tables into automated IMS processing.

Acknowledgments

The methodologies and tools presented here were developed in part in an effort supported by the Office of Naval Research to investigate whether signals from infrasound ground-truth events could be

inverted to obtain information about the atmosphere, i.e., ground-to-space infrasound acoustic tomography, such as is currently in routine use in oceanography and seismology.

References

Arrowsmith, S.J., Drob, D.P., Hedlin, M.A.H., and Edwards, W. (2007), *A joint seismic and acoustic study of the Washington State bolide: observations and modeling*, J. Geophys. Res.-Atmos *112*.

Arrowsmith, S.J., Whitaker, R., Taylor, S.R., Burlacu, R., Stump, B.W., Hedlin, M.A.H., Randall, G., Hayward, C., and Revelle, D.O. (2008), *Regional monitoring of infrasound events using multiple arrays*: *application to Utah and Washington State*, Geophys. J. Int. *175*, 291–300.

Bechtold, P., Kohler, M., Jung, T., Doblas-Reyes, F., Leutbecher, M., Rodwell, M.J., Vitart, F., and Balsamo, G. (2008), *Advances in simulating atmospheric variability with the ECMWF model: from synoptic to decadal time-scales*, Quart. J. Roy. Meteorol. Soc. *134*, 1337–1351.

Brown, D.J., Katz, C.N., Le Bras, R., Flanagan, M.P., Wang, J., and Gault, A.K. (2002a), *Infrasonic signal detection and source location at the Prototype International Data Centre*, Pure Appl. Geophys. *159*, 1081–1125.

Brown, P., Spalding, R.E., ReVelle, D.O., Tagliaferri, E., and Worden, S.P. (2002b), *The flux of small near-Earth objects colliding with the Earth*, Nature *420*, 294–296.

Cansi, Y. (1995), *An Automatic Seismic Event Processing for Detection and Location—the PMCC Method*, Geophys. Res. Lett *22*, 1021–1024.

Christie, D.R., Veloso, J.A.V., Campus, P., Bell, M., Hoffmann, T., Langlois, A., Martysevich, P., Demirovic, E., and Carvalho, J. (2001), *Detection of atmospheric nuclear explosions: the infrasound component of the International Monitoring System*, Kerntechnik *66*, 96–101.

Chunchuzov, I.P. (2004), *Influence of internal gravity waves on sound propagation in the lower atmosphere*, Meteorol. Atmos. Phys. *85*, 61–76.

Courtier, P., Andersson, E., Heckley, W., Pailleux, J., Vasiljevic, D., Hamrud, M., Hollingsworth, A., Rabier, E., and Fisher, M. (1998), *The ECMWF implementation of three-dimensional variational assimilation (3D-Var). I: Formulation*, Quart. J. Roy. Meteorol. Soc. *124*, 1783–1807.

Drob, D., Emmert, J.T., Crowley, G., Picone, J.M., Shepherd, G.G., Skinner, W., Hays, P., Niciejewski, R.J., Larsen, M., She, C.Y., Meriwether, J.W., Hernandez, G., Jarvis, M.J., D. P. Sipler, Tepley, C.A., O'Brien, M.S., Bowman, J.R., Wu, Q., Murayama, Y., Kawamura, S., Reid, I.M., and Vincent, R.A. (2008), *An Empirical Model of the Earth's Horizontal Wind Fields: HWM07*, J. Geophys. Res.-Space Phys., in press.

Drob, D.P., Picone, J.M., and Garces, M. (2003), *Global morphology of infrasound propagation*, J. Geophys. Res.-Atmos. *108*.

Edwards, W.N. and Hildebrand, A.R. (2004), *SUPRACENTER: Locating fireball terminal bursts in the atmosphere using seismic arrivals*, Meteor. & Planet. Sci. *39*, 1449–1460.

Evers, L.G. and Haak, H.W. (2007), *Infrasonic forerunners: Exceptionally fast acoustic phases*, Geophys. Res. Lett. *34*.

Forbes, J.M., Zhang, X.L., Talaat, E.R., and Ward, W. (2003), *Nonmigrating diurnal tides in the thermosphere*, J. Geophys. Res.-Space Phys. *108*.

Fritts, D.C. and Isler, J.R. (1994), *Mean motions and tidal and 2-day structure and variability in the mesosphere and lower thermosphere over Hawaii*, J. Atmos. Sci. *51*, 2145–2164.

Garces, M.A., Hansen, R.A., and Lindquist, K.G. (1998), *Traveltimes for infrasonic waves propagating in a stratified atmosphere*, Geophys. J. Internat. *135*, 255–263.

Georges, T.M. and Beasley, W.H. (1977), *Refraction of infrasound by upper-atmospheric winds*, J. Acoust. Soc. Am. 61, 28-34.

Gossard, E.E. and Hooke, W.H. *Waves in the Atmosphere: Atmospheric Infrasound and Gravity Waves: Their Generation and Propagation* (Elsevier Scientific Pub. Co., Amsterdam; New York 1975).

Hedin, A.E., Fleming, E.L., Manson, A.H., Schmidlin, F.J., Avery, S.K., Clark, R.R., Franke, S.J., Fraser, G.J., Tsuda, T., Vial, F., and Vincent, R.A. (1996), *Empirical wind model for the upper, middle and lower atmosphere*, J. Atmos. Terre. Phys. *58*, 1421–1447.

Hedlin, M.A.H., Garces, M., Bass, H.E., Hayward, Herrin, G., Olson, G., and Wilson, C. (2002), *Listening to the secret sounds of the earth's atmosphere*, Eos Trans. AGU *83*, 564–565.

Herrin, E.T., Kim, T.S., and Stump, B.W. (2006), *Evidence for an infrasound waveguide*, Geophys. Res. Lett. *33*.

Kalnay, E., Kanamitsu, M., and Baker, W.E. (1990), *Global Numerical Weather Prediction at the National-Meteorological-Center*, Bull. Am. Meteor. Soc. *71*, 1410–1428.

Le Pichon, A., Antier, K., Cansi, Y., Hernandez, B., Minaya, E., Burgoa, B., Drob, D., Evers, L.G., and Vaubaillon, J. (2008a), *Evidence for a meteoritic origin of the September 15, 2007, Carancas crater*, Meteor. Planet. Sci. *43*, 1797–1809.

Le Pichon, A., Blanc, E., Drob, D., Lambotte, S., Dessa, J.X., Lardy, M., Bani, P., and Vergniolle, S. (2005), *Infrasound monitoring of volcanoes to probe high-altitude winds*, J. Geophy. Res.-Atmos. *110*.

Le Pichon, A., Garces, M., Blanc, E., Barthelemy, M., and Drob, D.P. (2002), *Acoustic propagation and atmosphere characteristics derived from infrasonic waves generated by the Concorde*, J. Acoust. Soc. Am. *111*, 629–641.

Le Pichon, A., Vergoz, J., Herry, P., and Ceranna, L. (2008b), *Analyzing the detection capability of infrasound arrays in Central Europe*, J. Geophys. Res.-Atmos. *113*, 9.

Le Pichon, A., Vergoz, J., Herry, P., and Ceranna, L. (2008c), *Analyzing the detection capability of infrasound arrays in Central Europe*, J. Geophys. Res.-Atmos. *113*.

Lieberman, R.S., Riggin, D.M., Ortland, D.A., Nesbitt, S.W., and Vincent, R.A. (2007), *Variability of mesospheric diurnal tides and tropospheric diurnal heating during 1997-1998*, J. Geophys. Res.-Atmos. *112*, 17.

Lighthill, M.J. *Waves in Fluids,* (Cambridge University Press, Cambridge [Eng.]; New York 1978).

Lingevitch, J.F., Collins, M.D., Dacol, D.K., Drob, D.P., Rogers, J.C.W., and Siegmann, W.L. (2002), *A wide angle and high Mach number parabolic equation*, J. Acoust. Soc. Am. 111, 729–734.

Manney, G.L., Kruger, K., Pawson, S., Minschwaner, K., Schwartz, M.J., Daffer, W.H., Livesey, N.J., Mlynczak, M.G., Remsberg, E.E., Russell, J.M., and Waters, J.W. (2008), *The evolution of the stratopause during the 2006 major warming: Satellite data and assimilated meteorological analyses*, J. Geophys. Res.-Atmos. *113*.

McLandress, C., Ward, W.E., Fomichev, V.I., Semeniuk, K., Beagley, S.R., McFarlane, N.A., and Shepherd, T.G. (2006), *Large-scale dynamics of the mesosphere and lower thermosphere: An analysis using the extended Canadian Middle Atmosphere Model*, J. Geophys. Res.-Atmos. *111*.

Menke, W. *Geophysical Data Analysis: Discrete Inverse Theory*, Rev. edn. (Academic Press, San Diego 1989).

Millet, C., Robinet, J.C., and Roblin, C. (2007), *On using computational aeroacoustics for long-range propagation of infrasounds in realistic atmospheres*, Geophys. Res. Lett. *34*.

Nemtchinov, I.V., Svetsov, V.V., Kosarev, I.B., Golub, A.P., Popova, O.P., Shuvalov, V.V., Spalding, R.E., Jacobs, C., and Tagliaferri, E. (1997), *Assessment of kinetic energy of meteoroids detected by satellite-based light sensors*, Icarus *130*, 259–274.

Ostashev, V.E., Chunchuzov, I.P., and Wilson, D.K. (2005), *Sound propagation through and scattering by internal gravity waves in a stably stratified atmosphere*, J. Acoust. Soc. Am. *118*, 3420–3429.

Picone, J.M., Hedin, A.E., Drob, D.P., and Aikin, A.C. (2002), *NRLMSISE-00 empirical model of the atmosphere: Statistical comparisons and scientific issues*, J. Geophys. Res.-Space Phys. *107*.

Pierce, A.D. (1967), *Guided infrasonic modes in a temperature- and wind-stratified atmosphere*, J. Acoust. Soc. Am. *41*, 597.

Press, W.H. *Numerical Recipes: The Art of Scientific Computing*, (Cambridge University Press, Cambridge; New York 1989).

Smith, A.K. (1996), *Longitudinal variations in mesospheric winds: Evidence for gravity wave filtering by planetary waves*, J. Atmos. Sci. *53*, 1156–1173.

(Received November 21, 2008, revised January 12, 2009, accepted April 21, 2009, Published online March 10, 2010)